Effect of pH on the Active Site of an Arg121Cys Mutant of the Metallo-β-lactamase from *Bacillus cereus*: Implications for the Enzyme Mechanism[†,‡]

Anna M. Davies,[§] Rodolfo M. Rasia,[||] Alejandro J. Vila,[||] Brian J. Sutton,*[,§] and Stella M. Fabiane[§]

Randall Division of Cell and Molecular Biophysics, King's College London, New Hunt's House, Guy's Campus, London Bridge, SE1 1UL, London, United Kingdom, and Molecular Biology Division, IBR (Instituto de Biología Molecular y Celular de Rosario), CONICET, and Biophysics Section, Facultad de Ciencias Bioquímicas y Farmacéuticas, Universidad Nacional de Rosario, Suipacha 531, (S2002LRK) Rosario, Argentina

Received October 27, 2004; Revised Manuscript Received January 14, 2005

ABSTRACT: The zinc-dependent metallo-β-lactamases are a group of bacterial enzymes that pose a threat to the future efficacy of present-day antibiotics. Their mechanism is poorly understood, and there are no clinically useful inhibitors. While most members of the group contain two tightly bound zinc ions in their active sites, the *Bacillus cereus* enzyme has a much lower affinity for its second zinc (Zn2), thought to be due to the presence of Arg121 immediately beneath the floor of the active site (cf. Cys/Ser/His121 in the bizinc enzymes). Crystal structures of the Arg121Cys mutant of the *B. cereus* 569/H/9 enzyme were solved at pH 7.0, 5.0, and 4.5, each in the presence of either 20 μM or 20 mM Zn^{2+} to generate the mono- and bizinc forms, respectively. Surprisingly, the structure of the active site was unaffected by the mutation; a network of ordered water molecules replaced the interactions made by the arginine side chain, and the occupancy of Zn2 appeared minimally changed. As the pH was lowered, Zn2 moved away from one of its ligands, Asp120, but was "tracked" by two others, Cys221 and His263. Furthermore, the hydroxide ion (and proposed nucleophile for β-lactam hydrolysis) was bound to Zn1 at pH 5 and above but absent at pH 4.5. This provides experimental evidence for an earlier proposed mechanism in which protonation of Asp120 and the Zn1-bound hydroxide are the two events that lead to the loss of activity at low pH.

β-lactamases are enzymes capable of hydrolyzing the cyclic amide bond of the β-lactam ring that is a structural feature of commonly used antibiotics such as penicillins, cephalosporins, and carbapenems. Hydrolysis inactivates these compounds, and β-lactamase production is an important contributor to the increasing problem of bacterial resistance to antibiotics (*3*, *4*).

Four classes of β-lactamase enzymes have been identified (*5*−*7*). Classes A, C, and D comprise the serine β-lactamases that rely on a catalytic serine residue for activity and for which a clinical inhibitor, clavulanic acid, is available (*8*). Class B is comprised of the metallo-β-lactamases that depend on Zn^{2+} ions for activity (*9*, *10*). While some progress has been made in identifying molecules that inhibit the class B enzymes (e.g., refs *11*−*14* and references therein), there are as yet no clinically useful inhibitors available. The increasing prevalence of the metallo-β-lactamases, combined with the lack of clinically effective inhibitors, is of increasing concern to the medical community (*3*, *15*).

The metallo-β-lactamase from *Bacillus cereus* belongs to the B1 subclass (*1*). Crystal structures for five enzymes from this subclass have been solved: BcII from *B. cereus* (*16*−*19*), BlaB from *Chryseobacterium meningosepticum* (*20*), CcrA from *B. fragilis* (*21*−*23*), IMP-1 from *Pseudomonas aeruginosa* (*24*), and VIM-2 from *P. aeruginosa* (PDB code 1KO3). These structures reveal a remarkable degree of similarity between their active sites. Each is capable of binding two Zn^{2+} ions, with identical residues contributing to metal-ion coordination: His116, 118, and 196 for the first Zn^{2+} ion (Zn1) and Asp120, Cys221, and His263 for the second Zn^{2+} ion (Zn2).

Despite these similarities, the affinity of the B1 subclass enzymes for Zn^{2+} ions differs. The CcrA and IMP-1 enzymes possess two high-affinity metal-binding sites (*25*, *26*), but BcII binds Zn1 and Zn2 with different affinities (*9*, *27*−*29*). BcII is active in the presence of either one or two Zn^{2+} ions, although full activity is achieved when both Zn^{2+} ions are bound. In contrast, in the CphA enzyme from *Aeromonas hydrophila* (subclass B2; *30*), binding of a second zinc ion inhibits activity.

[†] A.M.D. is funded by a King's College London School of Biomedical Sciences studentship. R.M.R. is supported by a graduate fellowship from CONICET. A.J.V. is a staff member from CONICET and an International Research Scholar of the Howard Hughes Medical Institute. The work at the University of Rosario was supported by a grant from ANPCyT.

[‡] Residue numbering is in accordance with the BBL standard numbering system (*1*). Atomic coordinates and structure factors have been deposited in the Protein Data Bank (*2*). Cm7, 2BFK; Cm5, 2BFL; Cm4.5ox, 2BFZ; Cm4.5, 2BG2; Cμ7ox, 2BGA; Cμ5ox, 2BG6; Cμ4.5ox, 2BG7; and Cμ4.5, 2BG8.

* To whom correspondence should be addressed: Randall Division of Cell and Molecular Biophysics, King's College London, New Hunt's House, Guy's Campus, London Bridge, SE1 1UL, London, U.K. Telephone: +44 (0) 20 7848 6423. Fax: +44 (0) 20 7848 6410. E-mail: brian.sutton@kcl.ac.uk.

[§] King's College London.

[||] IBR and University of Rosario.

10.1021/bi047709t CCC: $30.25
Published on Web 03/05/2005

It has been suggested that a positively charged arginine residue (Arg 121) located in the floor of the BcII active site is responsible for the reduced affinity for Zn2 (*17*, *21*, *22*). In CcrA, where two high-affinity metal-binding sites are present, residue 121 is a cysteine. While a Na^+ ion was tentatively identified in the active site of CcrA, close to the position occupied by the guanidinium group of Arg121 in BcII, its position is actually further away from the Zn2 site than Arg121 in BcII and it is not thought to exert any affect on Zn2 affinity as a result (*21*, *22*). Likewise, in IMP-1, with two high-affinity metal-binding sites, residue 121 is a serine and the NZ atom of a lysine residue present in the active site is also further away from Zn2 (*24*). The two other B1 subclass enzymes for which structures are known, VIM-2 (PBD code 1KO3) and BlaB (*20*), have an arginine at position 121. In these structures, Zn2 was refined with 80% occupancy and a temperature factor either similar to (VIM-2) or greater than (BlaB) that for Zn1.

To determine whether Arg121 is indeed responsible for the reduced affinity of the Zn2 site in BcII 569/H/9, an Arg121Cys mutant (hereafter R121C) has recently been characterized, with activity (k_{cat}) determined for benzylpenicillin hydrolysis in the presence of 20 μM and 1 mM Zn^{2+} over a pH range of 4.5−7 (*31*). We now present crystallographic data for both mono- and bizinc forms of the BcII R121C mutant over the same range of pH values. While the affinity for Zn2 in this mutant is comparable to the wild-type enzyme (*31*), significant structural changes were found to occur in the active site as the pH is lowered, which provide insights into the mechanism of this enzyme. Because the activity profile of the R121C mutant is very similar to that of wild-type BcII (*31*) and the Cys mutation itself did not cause any changes to the structure of the enzyme, especially in the conformations of neighboring residues, it is expected that the observed pH-dependent changes will also occur in the wild-type enzyme.

MATERIALS AND METHODS

Crystallization. Expression and purification of the R121C mutant has already been described (*31*). Crystals were grown using the hanging drop vapor diffusion method. The reservoir solution contained 700 μL of 100 mM Tris-HCl at pH 4.5−5, 70−75% (v/v) saturated $(NH_4)_2SO_4$, 1 mM DTT or 1 mM TCEP-HCl, 2 mM $ZnSO_4$, and 0.1% (w/v) NaN_3. The drops contained 1.5−5 μL of protein solution at a concentration of 2.7 mg/mL, to which an equal volume of reservoir was added. After 1 day, the drops were streak-seeded from a crystal of the wild-type enzyme grown as described previously (*18*). The drops were kept at a temperature of 291 K (±0.5 K). The crystals had a trigonal morphology and were up to 150 μm in length. Single crystals were harvested after a period of 2−4 months into mother liquor solution.

Crystal Soaking and Cryocooling. Once harvested, crystals were soaked for 1−2 h in solutions of 100 mM Tris-HCl, 75% (v/v) saturated $(NH_4)_2SO_4$ containing $ZnSO_4$, 1 mM DTT alone or additionally with 1 mM TCEP-HCl, and 0.1% (w/v) NaN_3. The concentration of $ZnSO_4$ in the soaking solutions was controlled to manipulate zinc occupancy in the active site, and the pH of the solutions was adjusted to pH 4.5, 5, or 7 (±0.2) (Note that crystals only grow at a pH of 4.5−5). Details for each soak are given in Table 1. The soaking solutions were exchanged with cryoprotectant solutions comprised of the soaking solution components and 18% (v/v) glycerol, after which the crystals were mounted in nylon loops and flash-cooled in liquid nitrogen.

Table 1: Crystal-Soaking Details

dataset/soak	pH (±0.2)	$ZnSO_4$ concentration	reducing agent
Cm7	7.0	20 mM	1 mM DTT
Cm5	5.0	20 mM	1 mM DTT
Cm4.5ox	4.5	20 mM	1 mM DTT
Cm4.5	4.5	20 mM	1 mM DTT + 1 mM TCEP-HCl
Cμ7ox	7.0	20 μM	1 mM DTT
Cμ5ox	5.0	20 μM	1 mM DTT
Cμ4.5ox	4.5	20 μM	1 mM DTT
Cμ4.5	4.5	20 μM	1 mM DTT + 1 mM TCEP-HCl

Data Collection and Processing. The data were processed with DENZO (*32*) and the CCP4 suite of programs (*33*). Data processing statistics are summarized in Table 2.

Structure Determination, Model Building, and Refinement. Structures were solved using 1BC2 as a starting model. All ions and solvent molecules were removed from the model, and Arg121 was mutated to Ala. Electron density was typically present for residues 34−59 and 66−291. In cases where electron density allowed further building of the main chain, residues were included as Gly or Ala, unless sufficient density was present for the entire side chain. Refinement was performed using CNS (*34*). Cycles of refinement were alternated with rounds of manual model building with QUANTA (*35*) using σ_A weighted $2|F_o| - |F_c|$ and $|F_o| - |F_c|$ electron density maps. All ligand topology and parameter files used for refinement were obtained from the HIC-Up database (*36*). Protein topology and parameter files distributed with CNS were edited to include values for oxidized Cys residues (CEA and CSD). A total of 5% of reflections was used to calculate the R_{free} value throughout the refinement process, with the exception of two final rounds of refinement where all reflections were used. The two NCS-related molecules of the asymmetric unit (termed A and B) were refined independently, and with the exception of residues adopting alternative conformations where an occupancy of 50% was assigned to each conformer, all atoms (including the Zn^{2+} ions) were refined with an occupancy of 100%. The final models were analyzed using PROCHECK (*37*), SFCHECK (*38*), and CNS (*34*). In all structures, Asp84 adopts a forbidden conformation, but this was also found in wild-type BcII. Refinement and final model statistics are summarized in Table 3. All figures were produced with PyMOL (*39*).

RESULTS

Structural Effects of the Cys Mutation. Superposition of the polypeptide backbone atoms of all refined structures with wild-type BcII (PDB code 1BC2) revealed that the Cys121 mutation had not caused any overall structural changes [e.g., root-mean-square deviation (rmsd) between structure Cm7 molecule B and 1BC2 is 0.38 Å]. Cys121 adopted the same conformation in all structures, and this was found to be the same as that adopted in CcrA (*21*, *22*). Because Arg121 in wild-type BcII is important for maintaining structural integrity in the active site by forming a salt bridge with Asp84 and a hydrogen bond with Asp120 (*18*), it is

Table 2: Data-Processing Statistics

dataset	Cm7	Cm5	Cm4.5ox	Cm4.5	Cμ7ox	Cμ5ox	Cμ4.5ox	Cμ4.5
beamline, synchrotron source	ID13, ESRF[a]	ID14−1, ESRF[a]	ID13, ESRF[a]	14.2, SRS[b]	9.6, SRS[b]	14.2, SRS[b]	ID13, ESRF[a]	14.1, SRS[b]
space group	$P3_121$	$P3_121$	$P3_121$	$P3_121$	$P3_121$	$P3_121$	$P3_121$	$P3_121$
unit cell dimensions (Å)	$a = b =$ 67.311 $c = 178.010$	$a = b =$ 67.535 $c = 178.712$	$a = b =$ 67.309 $c = 177.604$	$a = b =$ 67.300 $c = 177.183$	$a = b =$ 67.391 $c = 178.530$	$a = b =$ 67.866 $c = 178.470$	$a = b =$ 67.578 $c = 178.769$	$a = b =$ 67.250 $c =177.800$
resolution limit (Å)	2.0	1.8	2.3	2.4	2.9	2.3	2.1	2.5
number of unique reflections	37 787	43 889	20 328	18 697	10 943	21 917	28 092	16 423
outer shell (Å)	2.04−1.97	1.85−1.80	2.36−2.30	2.46−2.40	2.98−2.90	2.36−2.30	2.15−2.10	2.57−2.50
completeness (%), overall [outer shell]	99.9 [99.9]	98.7 [98.7]	98.1 [95.8]	99.0 [99.0]	99.4 [99.3]	99.9 [99.9]	98.9 [92.2]	98.5 [99.5]
multiplicity, overall [outer shell]	11 [9.9]	6.8 [4.9]	3.5 [3.5]	5.2 [5.2]	2.9 [3.0]	6.4 [6.5]	4.9 [3.8]	4.3 [4.3]
I/σ, overall [outer shell]	4.4 [1.1]	9.5 [3.6]	5.3 [1.6]	5.7 [1.8]	4.5 [1.7]	6.9 [3.2]	9.4 [4.0]	6.0 [2.2]
R_{sym} (%), overall [outer shell]	10.7 [55.4]	5.3 [18.5]	15.2 [51.0]	9.4 [36.8]	13.2 [37.7]	8.4 [22.2]	6.1 [18.3]	10.5 [32.4]
R_{anom} (%), overall [outer shell]	3.9 [25.2]	2.4 [10.5]	n/a	n/a	n/a	3.5 [9.2]	n/a	n/a

[a] ESRF, European Synchrotron Radiation Facility, Grenoble, France. [b] SRS, Synchrotron Radiation Source, Daresbury Laboratory, U.K.

Table 3: Refinement Statistics

dataset	Cm7	Cm5	Cm4.5ox	Cm4.5	Cμ7ox	Cμ5ox	Cμ4.5ox	Cμ4.5
resolution range (Å)	58.72−2.00	55.90−1.80	9.90−2.30	58.72−2.40	16.69−2.90	41.88−2.30	59.76−2.10	58.72−2.50
number of reflections per asymmetric unit	71 090	82 092	20 328	18 697	10 943	40 700	28 092	16 423
number of protein atoms	3443	3370	3359	3356	3357	3378	3358	3361
number of water molecules	515	494	369	304	216	304	348	288
average *B* factor for protein atoms (Å^2)	21.51	20.46	18.38	23.47	21.17	19.33	19.06	22.66
R_{cryst} (%) (all reflections)	17.21	18.28	18.19	17.87	18.56	18.21	19.04	18.49
R_{free} (%) (5% of reflections)	20.85	20.21	23.87	22.44	24.75	22.27	22.20	23.74
σ_A coordinate error (Å)	0.20	0.17	0.25	0.26	0.29	0.23	0.18	0.28
rmsd, bond lengths (Å)	0.007	0.006	0.007	0.007	0.007	0.006	0.008	0.007
rmsd, bond angles (deg)	1.39	1.34	1.37	1.32	1.39	1.34	1.34	1.33

remarkable that there are no significant structural changes in the active site of the R121C mutant, not even at residues Asp84 or Asp120.

Environment of Cys121. As expected, mutation of the larger, positively charged Arg residue to Cys created a cavity in the floor of the active site of the BcII mutant. In CcrA, a possible Na^+ ion adjacent to the naturally occurring Cys121 lies close to the position occupied by the guanidinium group of Arg121 in BcII (*21*, *22*). No Na^+ ion was detected in the BcII R121C structure, and instead, a network of water molecules populates this cavity. In particular, a water molecule was identified in a position equivalent to either the NH1 or NH2 atoms of Arg121 (Figure 1), forming hydrogen bonds with Ser69 (Oγ), Asp120 (Oδ2), and Gly262 (carbonyl oxygen) and preserving the architecture of the active-site floor. Nevertheless, the lengths of these hydrogen bonds (average 3.0 Å) and the temperature factors of the water molecules [average 40 Å^2, compared with 23 Å^2 for the guanidinium group atoms in wild-type BcII (1BC2, 2BC2, 3BC2, and 1BVT) and 10 Å^2 for Na^+ in CcrA from *B. fragilis* (1ZNB and 2BMI)] implies that there may be less rigidity in the active site of the mutant enzyme.

The Active Site: Cm7. At pH 7, the optimum for BcII activity, and with a $ZnSO_4$ concentration of 20 mM, the active site of the R121C mutant contains two Zn^{2+} ions (Figure 2A). Zn1 is coordinated by His116, 118, and 196 and a water molecule/hydroxide (labeled Wat1) in a tetrahedral arrangement, and Zn2 is coordinated in a distorted trigonal bipyramidal arrangement by Asp120, Cys221, His263, Wat1, and either a glycerol molecule (glycerol 8, molecule A) or a second water molecule (W362, molecule B). Given the very short Zn−O distances of 1.89 and 1.99 Å (Table 4), Wat1 is almost certainly an hydroxide ion, as discussed earlier in relation to the wild-type structure (*18*). Wat1 is more symmetrically placed in this structure than in wild-type BcII (Table 4), but this is because the lower pH of the latter (pH 5.4) causes movement of Zn2 away from Zn1, as will be described below for the mutant structures.

The temperature factors for Zn2 in Cm7 (52 and 49 Å^2 in molecules A and B) were higher than those for Zn1 (both 22 Å^2), as seen in wild-type BcII (*17*, *18*). In our studies, we have set all zinc ion occupancy values to 100% and refined their temperature factors. This provides a combined measure of the degree of mobility and level of occupation at each site. The Zn1 and Zn2 temperature factors are therefore consistent with the lower affinity for Zn2 (*18*). Furthermore, because the temperature factor for Zn1 (22 Å^2) is almost identical to the average temperature factor for protein atoms in the structure (21.5 Å^2), this demonstrates 100% occupancy at this site.

Cm5. At pH 5 and a $ZnSO_4$ concentration of 20 mM, the active site also contains two Zn^{2+} ions (Figure 2B). Zn1 coordination was unchanged, but at the Zn2 site, the distance to Asp120 Oδ2 had increased (3.91 and 3.38 Å in molecules

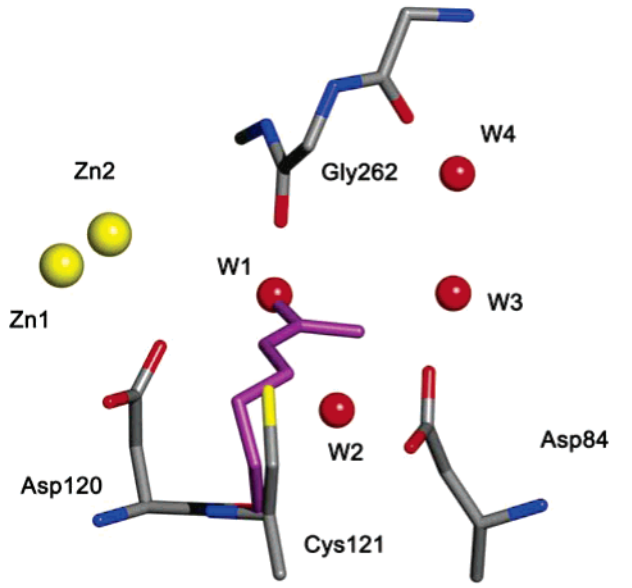

FIGURE 1: Active-site floor of the R121C mutant. The cavity created by the mutation, immediately underneath the active site, is populated by water molecules (red spheres, W1−4) as shown here for structure Cm7 molecule B. Some variation is seen in the other structures, but a water molecule (W1) lies close to the position occupied by the NH2 atom of Arg121 in wild-type BcII, forming hydrogen bonds to the other water molecules and to Ser69 (Oγ; not shown), Asp120 (Oδ2), and Gly262 (carbonyl oxygen). The position of Arg121 in wild-type BcII (1BC2 molecule A) is shown in purple. Zn1 and Zn2 are indicated by yellow spheres.

A and B, compared with 2.59 and 2.84 Å at pH 7). These increases are substantially greater than the combined σ_A coordinate error in the two structures (0.37 Å) and mean that Asp120 can no longer act as an effective ligand for Zn2. In contrast, the Zn2−Sγ (Cys221) and Zn2−Nϵ2 (His263) distances are unaltered with the change in pH, and these ligands track the movement of Zn2 (Table 4).

While the temperature factors for Zn1 at pH 5 (30 and 24 Å^2) are comparable with those at pH 7, the Zn2 values are much higher (82 and 119 Å^2; Table 5). This most likely reflects a lower occupancy of Zn2 caused by a partial oxidation of Cys221, because in the Cm4.5 structure in which no oxidation occurs (see below), the Zn2 occupancies are the same as those at pH 7. Despite possible partial oxidation of Cys221 in this structure, tracking of Zn2 is still observed, because a fraction of molecules in the crystal still contains Zn2 and Cys221 in its reduced form.

Cm4.5ox. At pH 4.5, despite the presence of 1 mM DTT, Cys221 was clearly oxidized with two additional oxygen atoms and was refined as *S*-cysteinesulfinic acid (CSD) in molecule A, as shown in Figure 2C, and as *S*-hydroxy-cysteine, with one additional oxygen atom, in molecule B. Only Zn1 was present in each molecule. While its protein ligands were unchanged from pH 7, Wat1 was missing from both molecules.

Cm4.5. Because DTT failed to protect Cys221 against oxidation at lower pH, TCEP-HCl was also added, and this successfully maintained Cys221 in the reduced state. At pH 4.5 in the presence of 20 mM $ZnSO_4$ and 1 mM TCEP-HCl, both Zn1 and Zn2 were present (Figure 2D), with temperature factors comparable to those at pH 7 (Table 5). However, Wat1 was still absent at this pH. Instead, a glycerol molecule (in molecule A) and a chloride ion (in molecule B, Figure 2D) bridged the Zn ions, although not at the same location as Wat1 (Zn1−Cl$^-$, 2.76 Å; Zn2−Cl$^-$, 3.12 Å).

Zn2 was again found to have moved away from Zn1 and Asp120 (Zn2−Oδ2, 3.79 Å in molecule A and 3.81 Å in molecule B; Table 4), and Cys221 and His263 again tracked this movement. This shift in Zn2 position at low pH is shown in Figure 3.

Cμ7ox. At a Zn^{2+} concentration of 20 μM, only one zinc ion (Zn1) was found in the active site (Figure 4A), with the same coordination as in the bizinc structures. Cys221 was found to be oxidized (CSD species in Figure 4A), probably as a result of crystallization at lower pH before adjustment to pH 7. This structure is important because it demonstrates that, in the absence of Zn2, Wat1 is bound to Zn1 exactly as in the bizinc structure at this pH (Cm7 structure; Figure 2A).

Cμ5ox. At pH 5 with a $ZnSO_4$ concentration of 20 μM and only 1 mM DTT as a reducing agent, Cys221 was again oxidized with only Zn1 present in the active site (Figure 4B). Its coordination, including Wat1, was exactly the same as for the monozinc structure at pH 7.0.

Cμ4.5ox. At pH 4.5, 20 μM $ZnSO_4$, and 1 mM DTT, Cys221 was oxidized to *S*-hydroxy-cysteine in both molecules (CEA in Figure 4C) and only Zn1 was present. In molecule A, Wat1 was found with a high-temperature factor (40 Å^2), while in molecule B, it was absent altogether (Figure 4C), consistent with the Cm4.5 and Cm4.5ox structures. There was however a slight increase in the Zn1−ligand distances in this structure (Table 4), and also in the temperature factors for Zn1 (Table 5), not seen in the Cm4.5 structures nor Cμ4.5 (see below). Interestingly, His263 adopted an alternative conformation in this structure, with the side-chain rotated away from the active site (Figure 4C). This has already been observed in monozinc wild-type structures (Fabiane, unpublished; PDB code 2BC2) and is therefore unrelated to the mutation.

Cμ4.5. Addition of 1 mM TCEP-HCl at pH 4.5 with 20 μM $ZnSO_4$ prevented oxidation of Cys221 in molecule B but not in molecule A, and while both molecules bound only Zn1, Wat1 was present in molecule A but absent from B (Figure 4D; as in Cμ4.5ox). The temperature factors for Zn1 were lower and the ligand distances were shorter than those in Cμ4.5ox, in line with those found in all of the other structures (Tables 4 and 5).

DISCUSSION

Zn^{2+} Occupancy in the Active Site. While some members of the metallo-β-lactamase family contain two tightly bound zinc ions, BcII is active with a single zinc ion (Zn1) liganded by three histidine residues and the presumed nucleophilic water/hydroxide moiety (here termed Wat1). Activity is enhanced when the second site (Zn2) is occupied, bound by Asp120, Cys221, and His263, but its role in the mechanism is unknown. Because the two zinc-binding sites in BcII have very different macroscopic binding constants (*9*, *27*, *40*), we have been able to determine structures with either one or two zinc ions bound by altering the zinc concentration. Recently, it has been suggested that the active site of monozinc BcII contains a single Zn^{2+} ion equally distributed between the Zn1 and Zn2 sites (*40*), but we have found no evidence for this in the crystal structures. In all of the

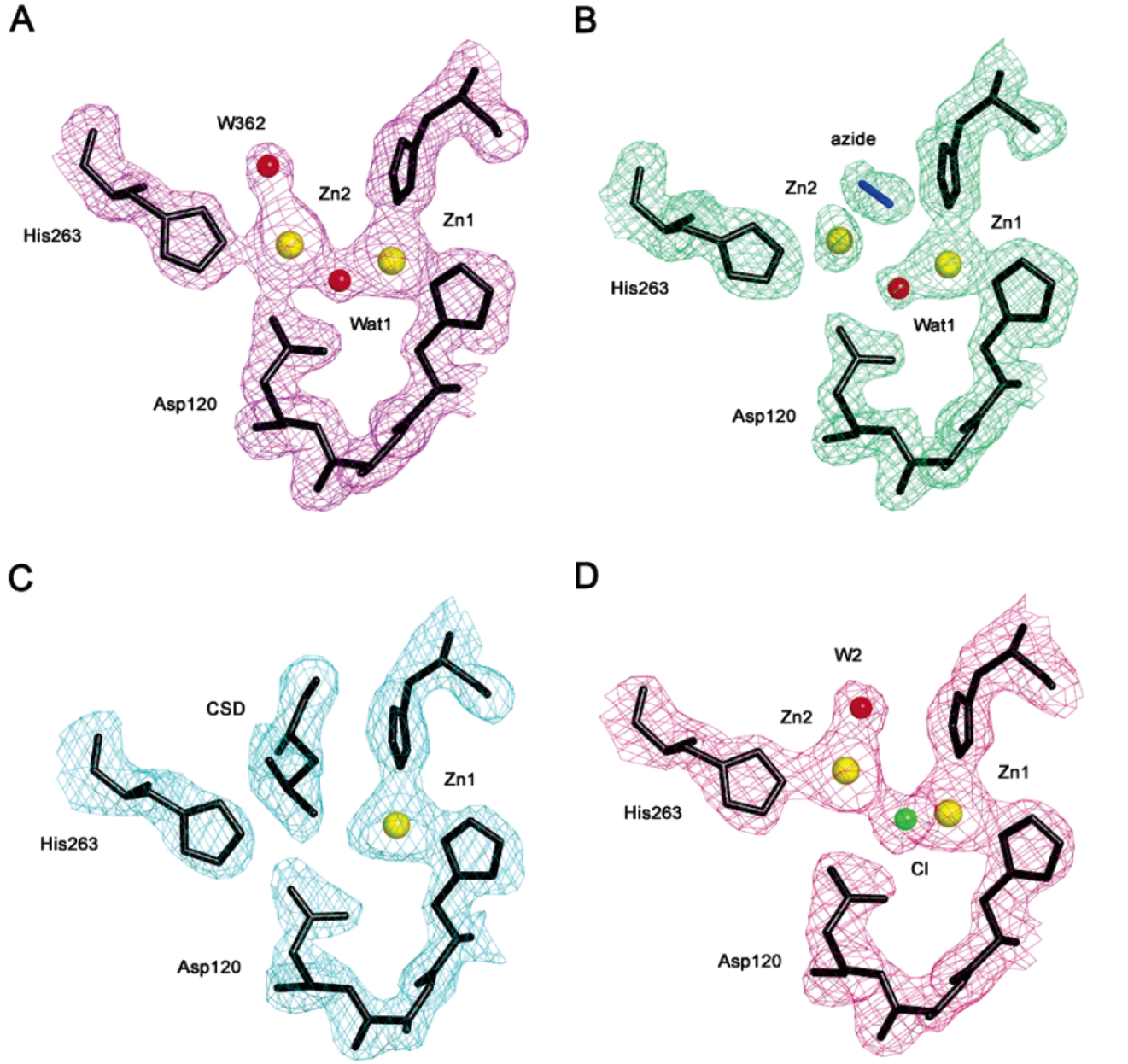

FIGURE 2: Electron density for the 20 mM Zn^{2+} R121C BcII structures. (A) Cm7 molecule B. Density is present for two Zn^{2+} ions. Zn1 is coordinated by three His ligands and Wat1. Zn2 is coordinated by Asp120, Cys221 (not shown), His263, Wat1, and W362. Density is contoured at 1.0σ. (B) Cm5 molecule B. Coordination of Zn1 is the same as in Cm7. Zn2 is coordinated by Cys221 (not shown), His263, Wat1, and an azide ion. Density is contoured at 1.0σ. (C) Cm4.5ox molecule A. Zn1 is coordinated by three His ligands, but Wat1 is absent. Cys221 is oxidized to CSD (two oxygen atoms), and His263 adopts the "in" conformation. Density is contoured at 1.0σ. (D) Cm4.5 molecule B. Zn1 is coordinated by three His ligands, but Wat1 is absent, replaced by a Cl^- ion that bridges Zn1 and Zn2. Coordination of Zn2 is completed by Cys221 (not shown), His263, and W2. Density is contoured at 1.25σ. Color code: Zn^{2+} (yellow), water (red), Cl^- (green), azide (blue), and protein atoms (black). All density is shown using σ_A weighted $2F_{obs} - F_{calc}$ electron density maps. For clarity, His116 is not shown.

structures reported here, both Zn1 and Zn2 were refined assuming an occupancy of 100%. The temperature factors (which cannot be refined independently of occupancy at this resolution) therefore reflect a combined measure of the degree of mobility and level of occupation at each site. Temperature factors close to 21.5 Å^2, the average value for the protein atoms of the structure, therefore correspond to approximately 100% occupancy. Higher values (and potentially lower occupancy) are recorded for some of the monozinc structures (Table 5), but in none of these is density detectable at the Zn2 site that would suggest exchange. In the bizinc structures, Zn2 temperature factors are higher (Table 5), as observed in earlier BcII structures (*17*, *18*), indicative of a lower occupancy and/or greater mobility at this site, but the low temperature factors for Zn1 in all of these bizinc structures imply full occupancy at that site and also preclude exchange.

Role of Arg121. It has been suggested that this arginine residue, lying immediately below the Zn2 site, is responsible for the lower affinity for the second zinc ion, because in BcII, VIM-2, and BlaB, there is crystallographic evidence for lower occupancy. In contrast, CcrA and IMP-1 have two high-occupancy Zn sites and residue 121 is cysteine and serine, respectively. It was surprising, therefore, that the R121C BcII mutant displayed affinities for Zn1 and Zn2 that were minimally changed from those of the wild type (*31*).

Table 4: Active-Site Interatomic Distances Compared to 1BC2 (Å)

	1BC2		Cm7		Cm5		Cm4.5ox		Cm4.5		Cμ7ox		Cμ5ox		Cμ4.5ox		Cμ4.5	
	A	B	A	B	A	B	A	B	A	B	A	B	A	B	A	B	A	B
Zn1−Nε2 (His116)	2.27	2.24	2.11	2.18	2.22	2.24	2.08	2.24	2.21	2.28	2.03	2.22	2.17	2.32	2.57	2.61	2.35	2.25
Zn1−Nδ1 (His118)	1.95	2.16	1.86	2.02	2.01	2.06	1.95	2.16	1.98	2.21	1.96	2.01	2.10	2.19	2.41	2.74	2.04	2.46
Zn1−Nε2 (His196)	2.00	2.11	2.06	2.10	2.07	2.12	2.20	2.11	2.04	2.15	2.08	2.09	2.31	2.08	2.53	2.35	2.07	2.13
Zn1−Wat1	1.90	1.90	1.89	1.99	2.08	2.04					2.07	2.07	2.16	2.12	2.19		2.29	
Zn1−Zn2	3.65	4.36	3.63	3.59	4.25	4.16			3.96	4.09								
Zn2−Wat1	2.48	3.06	2.13	2.33	2.97	2.82												
Zn2−Oδ2 (Asp120)	2.75	2.90	2.59	2.84	3.91	3.38			3.79	3.81								
Zn2−Sγ (Cys221)	1.91	1.98	2.37	2.15	2.24	2.21			2.44	2.46								
Zn2−Nε2 (His263)	2.59	2.45	2.50	2.49	2.52	2.24			2.44	2.32								
Wat1−Oδ1 (Asp120)	2.79	2.84	2.60	2.75	2.61	2.62					2.87	2.97	2.68	2.50	3.01		2.63	

Table 5: Temperature Factors for Zn^{2+} Ions (Å^2)

	Zn1	Zn2		Zn1	Zn2
Cm7 (A, B)	22, 22	52, 49	Cμ7ox (A, B)	24, 27	
Cm5 (A, B)	30, 24	82, 119	Cμ5ox (A, B)	29, 28	
Cm4.5ox (A, B)	21, 18		Cμ4.5ox (A, B)	53, 49	
Cm4.5 (A, B)	26, 24	47, 43	Cμ4.5 (A, B)	28, 37	

However, the temperature factors of the Cm7 and Cm4.5 structures show that the occupancy of Zn2 is either similar to or slightly greater than that in wild-type BcII (*18*). It is therefore possible that Arg121 may indeed play a role in affecting Zn2 affinity.

Arg121 appears to contribute to the orientation of Asp120 in wild-type BcII (*17*, *18*). It was therefore a further surprise to find the conformation of Asp120 unchanged in all of the R121C mutant structures solved, but a network of water molecules populating the cavity created by the mutation formed equivalent hydrogen bonds to Asp120. Even as the pH was lowered, Asp120 remained equally well-defined, implying that its protonation state (as discussed below) rather than its conformation was responsible for any loss of enzyme activity and affinity for Zn2. However, Arg121 may affect the pK_a of Asp120. Mutation of Arg121 to Cys may account for the shift of the acidic limb of the pH rate profile of the R121C mutant (*31*); the presence of arginine may thus serve to extend the useful pH range of the enzyme.

Oxidation of Cys221. Attention was first drawn to the oxidation of this active-site residue and Zn2 ligand when the structure of the apo form of BcII was solved at 2.5 Å resolution (*17*); oxidation was subsequently observed in monozinc BcII structures (PBD codes 2BC2 and 3BC2) and the VIM-2 metallo-β-lactamase from *P. aeruginosa* (1KO2). The process of Cys221 oxidation is not thought to abolish enzyme activity. When crystals of the R121C mutant were treated in a manner similar to those later observed to contain oxidized Cys221 and then soaked in a solution containing the chromophoric substrate nitrocefin, they were found to contain an active enzyme.

While all of the bizinc structures reported here contain an unoxidized Cys221, the converse is not true; not all of the monozinc structures contain an oxidized Cys221. The fact that, in the Cμ4.5 structure, Cys221 is oxidized in one molecule but not in the other, while both contain only one zinc ion, implies that it is not oxidation of this residue that causes the loss of Zn2. Instead, it is the loss of Zn2 from the active site that leaves Cys221 vulnerable to oxidation. This observation is consistent with the conclusions of Carfi et al. (*17*).

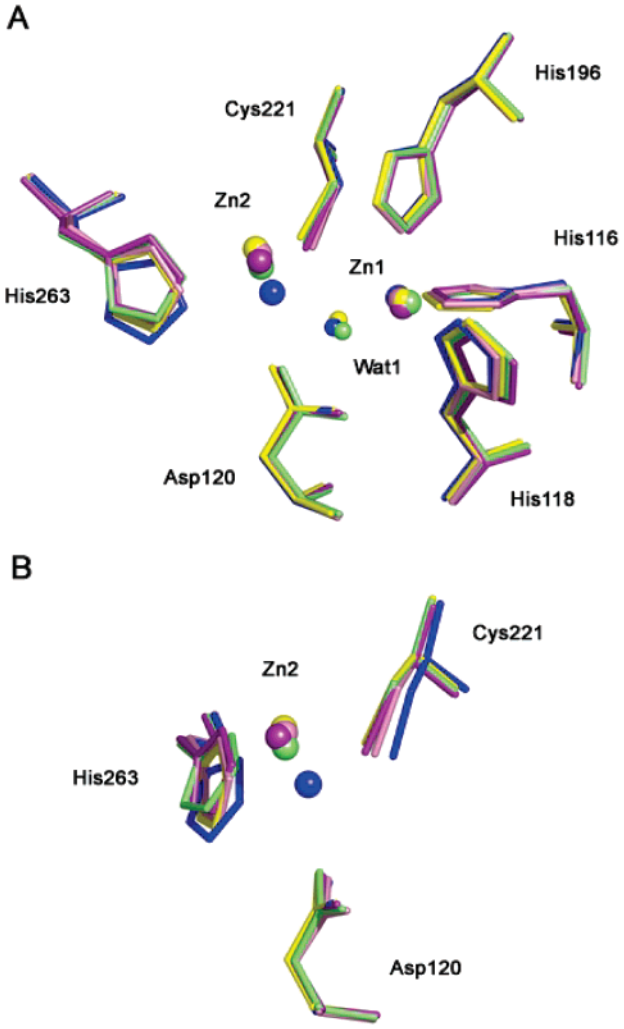

FIGURE 3: Shift in position of Zn2 at lower pH. (A) Superposition of the Cm5 and Cm4.5 structures on Cm7 (on the basis of all Cα positions) reveals that, while Zn1 and its ligands superpose well, Zn2, Cys221, and His263 do not. (B) Same as in A, viewed after rotation by ~90° clockwise about a vertical axis in the plane of the paper. Cys221 and His263 clearly "track" the movement of Zn2 away from the active site in Cm5 and Cm4.5. Color code: Cm7 molecule A (blue), Cm5 molecule A (yellow), Cm5 molecule B (green), Cm4.5 molecule A (pink), and Cm4.5 molecule B (purple).

Effect of pH on the Active Site. Lowering the pH from 7 to 4.5 causes a loss of enzyme activity (*31*, *41*, *42*), and the structures reported here reveal that, while there are only very small if any changes at the Zn1 site, there are very significant and progressive changes involving both Zn2 and the nucleophilic water/hydroxide (Wat1). Zn1 temperature factors and

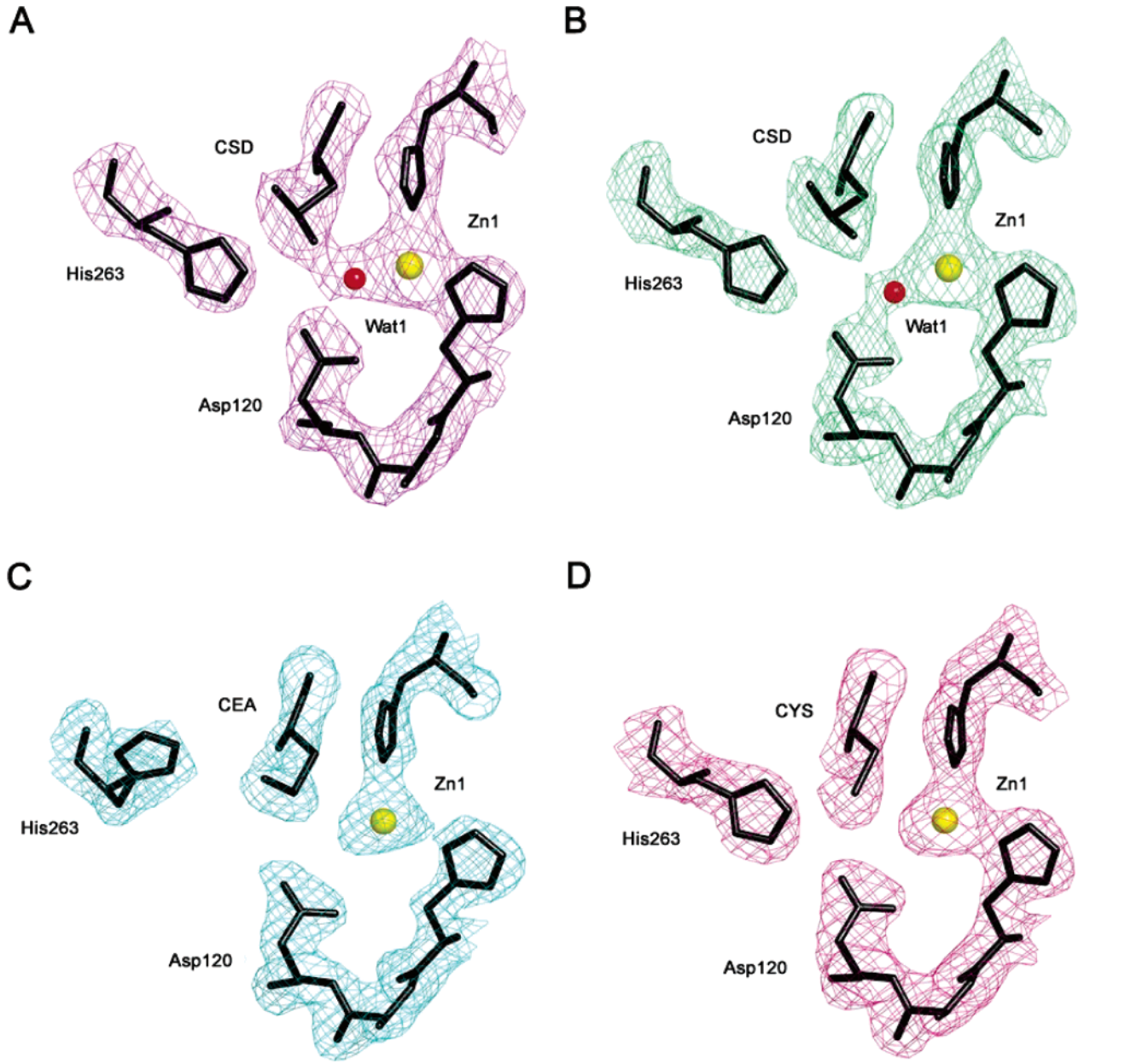

FIGURE 4: Electron density for the 20 μM Zn^{2+} R121C BcII structures. (A) Cμ7ox molecule A. Density is present for Zn1 and Wat1. Cys221 is oxidized to CSD (two oxygen atoms), and His263 adopts the "in" conformation. Density is contoured at 1.1σ. (B) Cμ5ox molecule B. Coordination of Zn1 is the same as in Cμ7ox. Cys221 is again oxidized to CSD, with His263 adopting the "in" conformation. Density is contoured at 1.0σ. (C) Cμ4.5ox molecule B. Zn1 is present, but Wat1 is absent. Cys221 exists as *S*-hydroxy-cysteine (CEA; one oxygen atom), and His263 adopts the "out" conformation. Density is contoured at 1.0σ. (D) Cμ4.5 molecule B. Zn1 is present, but Wat1 is absent. Cys221 is unoxidized, and His263 adopts the "in" conformation. Density is contoured at 1.0σ. Color code: Zn^{2+} (yellow), water (red), and protein atoms (black). All density is shown using σ_A weighted $2F_{obs} - F_{calc}$ electron-density maps. For clarity, His116 is not shown.

ligand distances are essentially the same in all of the bizinc structures (Tables 4 and 5), and although some of the monozinc structures show higher Zn1 temperature factors and ligand distances at pH 4.5, this is more pronounced in the oxidized structure (Cμ4.5ox) than that in the unoxidized structure (Cμ4.5), suggesting that it may not simply be a pH effect.

The effect on Zn2, however, is a progressive shift away from Zn1 and Asp120 as the pH is lowered. This can be seen in the comparison of the bizinc structures in Figure 3, and at pH 4.5, the Zn2−Oδ2 (Asp120) distances are almost 4 Å, too long for a metal−ligand bond, compared with 2.8−2.9 Å at pH 7 (Table 4). These shifts in the position of Zn2 are accompanied by corresponding shifts in two of its ligands, Cys221 and His263, which thus "track" the movement of Zn2 (Figure 3 and Table 4). Asp120, in contrast, remains fixed. This strongly suggests that protonation of Asp120 is the cause of these pH-dependent changes in the Zn2 position and argues against an earlier proposition that protonation of Cys221 and/or His263 might be the cause of the affinity changes at the Zn2 site (*17*).

The other pH-dependent change involves Wat1, which is still present in the bizinc structure at pH 5 (Figure 2B) but lost at pH 4.5 (parts C and D of Figure 2; in the latter structure, it is replaced by a chloride ion, presumably required to bridge the two zinc ions, and by glycerol in the other

molecule in the asymmetric unit). In the monozinc structures, Wat1 is similarly present at pH 5 (Figure 4B) but lost at pH 4.5 (parts C and D of Figure 4). Indeed, the Zn1−Wat1 distance progressively increases from 2.07 to 2.29 Å as the pH decreases from 7 to 4.5 (Table 4). Although these individual shifts are less than the coordinate error, the trend is consistent with protonation of Wat1/hydroxyl ion. A glycerol molecule bridging the two zinc ions was observed in the structure of FEZ-1, a B3 subclass metallo-β-lactamase from *Fluoribacter gormanii* (*43*), where it was suggested that the glycerol molecule had displaced Wat1 from the active site. However, from the series of structures reported here, we conclude that Wat1 is protonated at lower pH and leaves the active site, replaced in some cases by an alternative species. (In fact, of the eight enzyme molecules determined at pH 4.5, with four crystal structures each with two molecules in the asymmetric unit, Wat1 was only present in molecules A of Cμ4.5ox and Cμ4.5, whereas Wat1 was present in all 16 molecules solved at pH 7 and 5.)

The structures reported here thus imply that the two most likely protonation events occurring at lower pH in BcII involve Asp120 and Wat1, with the former leading to a movement of Zn2 away from Zn1 and Asp120 and the latter leading to the loss of the presumed nucleophilic hydroxide moiety as a water molecule.

Correlation with a Proposed Mechanism for BcII. Bounaga et al. (*42*) have proposed a mechanism for BcII in which enzyme activity requires that both Wat1 and Asp120 are deprotonated, with the former acting as a nucleophilic hydroxide moiety and the latter acting as a general base, accepting a proton from the attached hydroxyl group. The pH rate profiles of both wild-type BcII (*42*) and the R121C mutant (*31*) show a gradient of 2 in the region between pH 4.5 and 7, indicating that two basic residues are essential for catalytic activity. [The pH rate profile for wild-type BcII was obtained by a plot of log k_{cat}/K_m for benzylpenicillin and cephaloridine hydrolysis over a pH range of 4−10.5, with a Zn^{2+} concentration 10-fold greater than that of the enzyme (*42*). The pH rate profile for the R121C mutant was obtained by a plot of k_{cat} for benzylpenicillin hydrolysis in the presence of 20 μM and 1 mM Zn^{2+} over a pH range of 4.5−7 (*31*).]

Bounaga et al. tentatively identified the basic species, each with a pK_a of ~5.6, as Wat1 and Asp120 (*42*). Although this is a high pK_a value for the latter, the crystallographic data presented here, in particular the movement of Zn2 away from Asp120 and the loss of Wat1 from the active site as the pH is lowered from 7 to 4.5, are consistent with these two assignments and support the notion that these are the two basic species essential for activity.

Although we have provided structural evidence for the identity of the two key species required for enzyme activity in BcII, the role of Zn2 in catalysis is still unclear. One suggestion is that it interacts with the substrate (*18*), and certainly, the movement of Zn2 at lower pH, as observed here in the R121C mutant, may interfere with this interaction. Alternatively, like Arg121, Zn2 may affect the pK_a of Asp120. Only the structure of a substrate complex will definitively answer this question.

ACKNOWLEDGMENT

We thank James Nicholson, Elizabeth Duke, Rob Kehoe, Mike Macdonald, and Miroslav Papiz for assistance during data collection at the SRS and Manfred Burghammer for assistance during data collection at the ESRF.

REFERENCES

1. Galleni, M., Lamotte-Brasseur, J., Rossolini, G. M., Spencer, J., Dideberg, O., Frère, J. M., and the Metallo-β-Lactamase Working Group (2001) Standard numbering scheme for class B β-lactamases, *Antimicrob. Agents. Chemother. 35*, 660−663.
2. Berman, H. M., Westbrook, J., Feng, Z., Gilliland, G., Bhat, T. N., Weissig, H., Shindvalov, I. N., and Bourne, P. E. (2000) The Protein Data Bank, *Nucleic Acids Res. 28*, 235−242.
3. Walsh, C. (2000) Molecular mechanisms that confer antibacterial drug resistance, *Nature 406*, 775−781.
4. Frère, J. M (1995) *Mol. Microbiol. 16*, 385−395.
5. Ambler, R. P. (1980) The structure of β-lactamases, *Philos. Trans. R. Soc. London, Ser. B 289*, 321−331.
6. Bush, K. (1989) Classification of β-lactamases: Groups 1, 2a, 2b, and 2b′, *Antimicrob. Agents Chemother. 33*, 264−270.
7. Bush, K. (1989) Classification of β-lactamases: Groups 2c, 2d, 2e, 3, and 4, *Antimicrob. Agents Chemother. 33*, 271−276.
8. Liras, P., and Rodríguez-Garcia, A. (2000) Clavulanic acid, a β-lactamase inhibitor: Biosynthesis and molecular genetics, *Appl. Microbiol. Biotechnol. 54*, 467−475.
9. Davies, R. B., and Abraham, E. P. (1974) Metal cofactor requirements of β-lactamase II, *Biochem. J. 143*, 129−135.
10. Wang, Z., Fast, W., Valentine, A. M., and Benkovic, S. J. (1999) Metallo-β-lactamase: Structure and mechanism, *Curr. Opin. Chem. Biol. 3*, 614−622.
11. Bounaga, S., Galleni, M., Laws, A. P., and Page, M. I. (2001) Cysteinyl peptide inhibitors of *Bacillus cereus* zinc β-lactamase, *Bioorg. Med. Chem. 9*, 503−510.
12. Toney, J. H., Hammond, G. G., Fitzgerald, P. M. D., Sharma, N., Balkovec, J. M., Rouen, G. P., Olson, S. H., Hammond, M. L., Greenlee, M. L., and Gao, Y. D. (2001) Succinic acids as potent inhibitors of plasmid-borne IMP-1 metallo-β-lactamase, *J. Biol. Chem. 276*, 31913−31918.
13. Mollard, C., Moali, C., Papamicael, C., Damblon, C., Vessilier, S., Amicosante, G., Schofield, C. J., Galleni, M., Frère, J. M., and Roberts, G. C. K. (2001) Thiomandelic acid, a broad spectrum inhibitor of zinc β-lactamases, *J. Biol. Chem. 276*, 45015−45023.
14. Siemann, S., Evanoff, D. P., Marrone, L., Clarke, A. J., Viswanatha, T., and Dmitrienko, G. I. (2002) *N*-Arylsulfonyl hydrazones as inhibitors of IMP-1 metallo-β-lactamase, *Antimicrob. Agents Chemother. 46*, 2450−2457.
15. Payne, D. J. (1993) Metallo-β-lactamases−A new therapeutic challenge, *J. Med. Microbiol. 39*, 93−99.
16. Carfi, A., Pares, S., Duée, E., Galleni, M., Duez, C., Frère, J. M., and Dideberg, O. (1995) The 3D structure of a zinc metallo-β-lactamase from *Bacillus cereus* reveals a new type of protein fold, *EMBO J. 14*, 4914−4921.
17. Carfi, A., Duée, E., Galleni, M., Frère, J. M., and Dideberg, O. (1998) 1.85 Å resolution structure of the zinc(II) β-lactamase from *Bacillus cereus*, *Acta Crystallogr., Sect. D 54*, 313−323.
18. Fabiane, S. M., Sohi, M. K., Wan, T., Payne, D. J., Bateson, J. H., Mitchell, T., and Sutton, B. J. (1998) Crystal structure of the zinc-dependent β-lactamase from *Bacillus cereus* at 1.9 Å resolution: Binuclear active site with features of a mononuclear enzyme, *Biochemistry 37*, 12404−12411.
19. Chantalat, L., Duée, E., Galleni, M., Frère, J. M., and Dideberg, O. (2000) Structural effects of the active site mutation cysteine to serine in *Bacillus cereus* zinc-β-lactamase, *Protein Sci. 9*, 1402−1406.
20. García-Sáez, I., Hopkins, J., Papamicael, C., Franceschini, N., Amicosante, G., Rossolini, G. M., Galleni, M., Frère, J. M., and Dideberg, O. (2003) The 1.5-Å Structure of *Chryseobacterium meningosepticum* zinc β-lactamase in complex with the inhibitor, D-captopril, *J. Biol. Chem. 278*, 23868−23873.
21. Concha, N. O., Rasmussen, B. A., Bush. K., and Herzberg, O. (1996) Crystal structure of the wide-spectrum binuclear zinc-β-lactamase from *Bacteroides fragilis*, *Structure 4*, 823−836.
22. Carfi, A., Duée, E., Paul-Soto, R., Galleni, M., Frère, J. M., and Dideberg, O. (1998) X-ray structure of the Zn^{II} β-lactamase from

Bacteroides fragilis in an orthorhombic crystal form, *Acta Crystallogr., Sect. D 54*, 47−57.
23. Fitzgerald, P. M. D., Wu, J. K., and Toney, J. H. (1998) Unanticipated inhibition of the metallo-β-lactamase from *Bacteroides fragilis* by 4-morpholineethanesulfonic acid (MES): A crystallographic study at 1.85 Å resolution, *Biochemistry 37*, 6791−6800.
24. Concha, N. O., Janson, C. A., Rowling, P., Pearson, S., Cheever, C. A., Clarke, B. P., Lewis, C., Galleni, M., Frère, J. M., Payne, D. J., Bateson, J. H., and Abdel-Meguid, S. S. (2000) Crystal structure of the IMP-1 metallo-β-lactamase from *Pseudomonas aeruginosa* and its complex with a mercaptocarboxylate inhibitor: Binding determinants of a potent, broad-spectrum inhibitor, *Biochemistry 39*, 4288−4298.
25. Crowder, M. W., Wang, Z., Franklin, S. L., Zovinka, E. P., and Benkovic, S. J. (1996) Characterization of the metal-binding sites of the β-lactamase from *Bacteroides fragilis*, *Biochemistry 35*, 12126−12132.
26. Laraki, N., Franceschini, N., Rossolini, G. M., Santucci, P., Meunier, C., de Pauw, E., Amicosante, G., Frère, G. M., and Galleni, M. (1999) Biochemical characterization of the *Pseudomonas aeruginosa* 101/1477 metallo-β-lactamase IMP-1 produced by *Escherichia coli*, *Antimicrob. Agents Chemother. 43*, 902−906.
27. Baldwin, G. S., Galdes, A., Hill, H. A. O., Smith, B. E., Waley, S. G., and Abraham, E. P. (1978) Histidine residues as zinc ligands in β-lactamase II, *Biochem. J. 175*, 441−447.
28. Baldwin, G. S., Galdes, A., Hill, H. A. O., Waley, S. G., and Abraham, E. P. (1980) A spectroscopic study of metal ion and ligand binding to β-lactamase II, *J. Inorg. Biochem. 13*, 189−204.
29. Orellano, E. G., Girardini, J. E., Cricco, J. A., Ceccarelli, E. A., and Vila, A. J. (1998) Spectroscopic characterisation of a binuclear metal site in *Bacillus cereus* β-lactamase II, *Biochemistry 37*, 10173−10180.
30. Hernandez Valladares, M., Felici, A., Weber, G., Adolph, H. W., Zeppezauer, M., Rossolini, G. M, Amicosante, G., Frère, J. M., and Galleni, M. (1997) Zn^{II} Dependence of the *Aeromonas hydrophila* AE036 metallo-β-lactamase activity and stability, *Biochemistry 36*, 11534−11541.
31. Rasia, R. M., and Vila, A. J. (2002) Exploring the role and the binding affinity of a second zinc equivalent in *B. cereus* metallo-β-lactamase, *Biochemistry 41*, 1853−1860.
32. Otwinowski, Z., and Minor, W. (1997) Processing of X-ray diffraction data collected in oscillation mode, *Methods Enzymol. 276*, 307−325.
33. CCP4, Collaborative Computational Project, Number 4 (1994) The CCP4 suite: Programs for protein crystallography, *Acta Crystallogr., Sect. D 50*, 760−763.
34. Brünger, A. T., Adams, P. D., Clore, G. M., DeLano, W. L., Gros, P., Grosse-Kunstleve, R. W., Jiang, J., Kuszewski, J., Nilges, M., Pannu, N. S., Read, R. J., Rice, L. M., Simonson, T., and Warren, G. L. (1998) Crystallography and NMR system: A new software suite for macromolecular structure determination, *Acta Crystallogr., Sect. D 54*, 905−921.
35. *QUANTA2000* (2000) Molecular Simulations Inc., San Diego, CA.
36. Kleywegt, G. J., and Jones, T. A. (1998) Databases in protein crystallography, *Acta Crystallogr., Sect. D 54*, 1119−1131.
37. Laskowski, R. A., MacArthur, M. W., Moss, D. S., and Thornton, J. M. (1993) PROCHECK—A program to check the stereochemical quality of protein structures, *J. Appl. Crystallogr. 26*, 283−291.
38. Vaguine, A. A., Richelle, J., and Wodak, S. J. (1999) SFCHECK: A unified set of procedures for evaluating the quality of macromolecular structure-factor data and their agreement with the atomic model, *Acta Crystallogr., Sect. D 55*, 191−205.
39. DeLano, W. L. (2002) *The PyMOL Molecular Graphics System*, DeLano Scientific, San Carlos, CA.
40. De Seny, D., Heinz, U., Wommer, S., Kiefer, M., Meyer-Klaucke, W., Galleni, M., Frère, J. M., Bauer, R., and Adolph, H. W. (2001) Metal ion binding and coordination geometry for wild-type and mutants of metallo-β-lactamase from *Bacillus cereus* 569/H/9, *J. Biol. Chem. 276*, 45065−45078.
41. Bicknell, R., and Waley, S. G. (1985) Cryoenzymology of *Bacillus cereus* β-lactamase II, *Biochemistry 24*, 6876−6887.
42. Bounaga, S., Laws, A. P., Galleni, M., and Page, M. I. (1998) The mechanism of catalysis and the inhibition of the *Bacillus cereus* zinc-dependent β-lactamase, *Biochem. J. 333*, 703−711.
43. García-Sáez, I., Mercuri, P. S., Papamicael, C., Kahn, R., Frère, J. M., Galleni, M., Rossolini, G. M., and Dideberg, O. (2003) Three-dimensional structure of FEZ-1, a monomeric subclass B3 metallo-β-lactamase from *Fluoribacter gormanii*, in native form and in complex with D-captopril, *J. Mol. Biol. 325*, 651−660.

BI047709T